Monthly Notices of the ROYAL ASTRONOMICAL SOCIETY

MNRAS **498,** 3852–3862 (2020) doi:10.1093/mnras/staa2636
Advance Access publication 2020 September 2

Accretion of galaxy groups into galaxy clusters

José A. Benavides [1]★ Laura V. Sales [2] and Mario. G. Abadi [1,3]

[1]*Instituto de Astronomía Teórica y Experimental, CONICET-UNC, Laprida 854, X5000BGR Córdoba, Argentina*
[2]*Department of Physics and Astronomy, University of California, Riverside, CA 92521, USA*
[3]*Observatorio Astronómico de Córdoba, Universidad Nacional de Córdoba, Laprida 854, X5000BGR Córdoba, Argentina*

Accepted 2020 August 24. Received 2020 July 29; in original form 2020 May 12

ABSTRACT

We study the role of group infall in the assembly and dynamics of galaxy clusters in ΛCDM. We select 10 clusters with virial mass $M_{200} \sim 10^{14}\,\mathrm{M}_{\odot}$ from the cosmological hydrodynamical simulation Illustris and follow their galaxies with stellar mass $M_{\star} \geq 1.5 \times 10^{8}\,\mathrm{M}_{\odot}$. A median of ∼38 per cent of surviving galaxies at $z = 0$ is accreted as part of groups and did not infall directly from the field, albeit with significant cluster-to-cluster scatter. The evolution of these galaxy associations is quick, with observational signatures of their common origin eroding rapidly in 1–3 Gyr after infall. Substructure plays a dominant role in fostering the conditions for galaxy mergers to happen, even within the cluster environment. Integrated over time, we identify (per cluster) an average of 17 ± 9 mergers that occur in infalling galaxy associations, of which 7 ± 3 occur well within the virial radius of their cluster hosts. The number of mergers shows large dispersion from cluster to cluster, with our most massive system having 42 mergers above our mass cut-off. These mergers, which are typically gas rich for dwarfs and a combination of gas rich and gas poor for $M_{\star} \sim 10^{11}\,\mathrm{M}_{\odot}$, may contribute significantly within ΛCDM to the formation of specific morphologies, such as lenticulars (S0) and blue compact dwarfs in groups and clusters.

Key words: galaxies: clusters: general – galaxies: dwarf – galaxies: elliptical and lenticular, cD – galaxies: groups: general – galaxies: interactions – galaxies: kinematics and dynamics .

1 INTRODUCTION

Galaxies are seldom uniformly distributed within galaxy clusters. Groups and substructures have been detected observationally in cluster surveys using positions and velocities (Conselice & Gallagher 1998; Gurzadyan & Mazure 1998; Biviano et al. 2002; Lisker et al. 2018; Iodice et al. 2019), gravitational lensing (Treu et al. 2003; Natarajan et al. 2009), and also in X-ray maps (Owers, Couch & Nulsen 2009a; Owers et al. 2009b; Zhang et al. 2009; Jauzac et al. 2016). Given the typically large velocity dispersion associated with galaxy clusters, $\sigma \simeq 500$–1000 km s^{-1}, the probability of such associations to spontaneously occur after the galaxies are embedded in the gravitational potential of the cluster is negligible. Such associations of galaxies must therefore have already fallen in together as single units during the assembly of their cluster hosts.

This type of group infall arises naturally in hierarchical formation models such as the ΛCDM, where structure and substructure are self-similar. This means that not only the mass distribution within the host halo has a nearly universal profile regardless of halo mass (Navarro, Frenk & White 1996, 1997), also the distribution of mass in substructures (i.e. satellites) that infall into those hosts can be described by a single function, provided that substructure masses are properly scaled by the host halo mass (Giocoli, Tormen & van den Bosch 2008; Giocoli et al. 2010; Yang et al. 2011). The latter is referred to as the 'unevolved satellite mass function' because it quantifies mass of substructure at infall and not at $z = 0$, which may depend on the host (see van den Bosch, Tormen & Giocoli 2005; Giocoli et al. 2008, for details). This self-similar behaviour in structure and infalling substructure follows in general for any model characterized by a scale-free power spectrum of perturbation (like the ΛCDM) combined with the scale-free nature of gravity.

It is possible to quickly explore what this universal unevolved satellite mass function means for the assembly of different hosts. Taking equation (2) in Giocoli et al. (2008), we find that ∼2 satellites are expected to infall with mass 10 per cent that of the host. Applied to the Milky Way (MW), this rightly predicts 1–2 subhaloes with infall mass $10^{11}\,\mathrm{M}_{\odot}$ comparable to that inferred for the Large Magellanic Cloud (LMC), the most massive satellite in the MW. This is in agreement with current estimates on the assembly history of the MW (Boylan-Kolchin et al. 2010; Busha et al. 2011; De Lucia 2012). If instead, one now applies this argument to a host halo like the Virgo cluster, assuming a virial mass $\sim 10^{14}\,\mathrm{M}_{\odot}$, it predicts that 1–2 subhaloes with halo mass $\sim 10^{13}\,\mathrm{M}_{\odot}$ are expected to infall during the assembly history. This large halo mass, comparable to low-mass groups of galaxies, will be hosting more than one single galaxy and demonstrates that group infall is a clear prediction of ΛCDM.

Considering lower mass subhaloes, the unevolved satellite mass function predicts ∼20 objects with halo mass ≥1 per cent that of the host. For a cluster-mass host like Virgo, this means about ∼20 MW-mass galaxies and above, with halo mass $\geq 10^{12}\,\mathrm{M}_{\odot}$. This seems not too far off from observed stellar mass functions in Virgo for galaxies with $M_{\star} \geq 10^{10}\,\mathrm{M}_{\odot}$ (Trentham & Hodgkin 2002; Rines & Geller 2008) or from statistical studies in SDSS for groups in this mass range (Yang, Mo & van den Bosch 2009). However, we have not

★ E-mail: jose.astroph@gmail.com

accounted for tidal disruption and stripping, which will tend to lower the number of galaxies that survive at $z = 0$ in this mass range. Therefore, some $\sim L_\star$ will be necessarily contributed from the larger mass groups with halo mass $\sim 10^{13}$ M$_\odot$.

Several studies have quantified the relevance of group accretion using simulations and semi-analytical models (Taylor & Babul 2004, 2005a, b; Berrier et al. 2009; McGee et al. 2009; Cohn 2012; De Lucia et al. 2012; Román & Trujillo 2017; Bahé et al. 2019). For example, using *N*-body only cosmological zoom-in simulations of clusters, Berrier et al. (2009) measured about 25 per cent of MW-mass objects in clusters must be accreted as satellites instead of centrals from the field. This fraction is unknown for lower mass dwarfs.

The connection between these theoretical predictions and observations is, however, not straightforward. After these groups of galaxies enter the gravitational potential of the cluster, tidal forces will act to disrupt the coherence of the group (Gonzalez-Casado, Mamon & Salvador-Sole 1994), eventually mixing and erasing the typical signatures of common origin in the group members, such as spatial proximity and low mutual velocities. The ability to reconstruct, in present-day observations, the presence of galaxy groups that fell in together will depend on three factors: (i) the typical time-scale for disruption of the groups, (ii) the assembly history of the cluster – early formation means more time for tides to disrupt the groups – and (iii) the multiplicity of the groups – having more galaxies allows for easier sampling of clustering in velocity or spatial scale.

The third point mentioned above is automatically addressed by studying fainter galaxies, as low-mass dwarfs dominate in numbers in any system. The situation for factors listed in (i) and (ii) is less clear. Previous work has indicated a large range of tidal disruption time-scales, going from a very rapid dissociation of the groups (Gonzalez-Casado et al. 1994; Lisker et al. 2018; Choque-Challapa et al. 2019) to expecting several Gyr (Vijayaraghavan, Gallagher & Ricker 2015). Partially, such discrepancies can be explained by the use of different definitions in the literature; for instance, when the system is considered tidally disrupted or the exact definition of what is a group or association of galaxies at infall. However, some consensus exists: when substructure in position or velocity is *observationally* detected, it is interpreted as a young accretion event, typically suggesting less than 1–2 Gyr since infall (Lisker et al. 2018).

Here, our comparison to the MW can be used again to build up intuition. A scaled-down version of group infall is observed in our own galaxy with the LMC, which is expected to have brought along several fainter dwarfs that cluster in phase space with the orbit of the LMC (D'Onghia 2008; Sales et al. 2011, 2017; Jethwa, Erkal & Belokurov 2016). Observationally, the identification of dwarfs associated with the LMC is facilitated by two factors. First, detection of dwarfs in the MW goes down to the ultra-faint limit $M_\star \sim 10^3$–10^4 M$_\odot$, allowing to sample several group members. Secondly, the Magellanic Clouds are on their first infall and have only recently fallen into the MW no more than 2 Gyr ago (Kallivayalil, van der Marel & Alcock 2006; Kallivayalil et al. 2013).

In extragalactic systems that are megaparsecs away, projection effects in conjunction with shallower galaxy surveys make the identification of groups more difficult. Take for instance nearby clusters like Virgo or Fornax, where exquisitely deep surveys are able to map dwarfs down to $M_\star \sim 10^6$–$10^{7.5}$ M$_\odot$ (Venhola et al. 2017; Ferrarese et al. 2020). This is still several orders of magnitudes brighter than is possible in the MW. Encouragingly, some evidence already exists, for example in the Virgo cluster, where samples of dwarfs with *r*-band magnitudes $-17 \geq M_r \geq -18$ show a skewed velocity distribution that has been attributed to a recent group infall event (Lisker et al. 2018). Moreover, both systems, Virgo and Fornax have also obvious ongoing group infall in their outskirts, with the M49 group and Fornax A examples, respectively (Binggeli, Tammann & Sandage 1987; Iodice et al. 2017; Su et al. 2019). However, the detection of older accretion events deeper into the potential well of the clusters and/or groups with smaller masses remains an observational challenge, complicating the direct comparison to theoretical predictions.

Could group infall also play a role in explaining the different properties of cluster galaxies versus those in the field? Galaxies in clusters typically show lower star formation rates, older stellar populations, and more spherically dominated morphologies than field counterparts with similar mass. How much of this transformation is due to the infalling group environment versus the cluster environment is unclear, but there is exciting observational evidence in favour of 'pre-processing' in groups being an important factor lowering the star formation of some galaxies already before they join the cluster(Mihos 2003; Vijayaraghavan & Ricker 2013; Roberts & Parker 2017; Sarron et al. 2019). Bear in mind that only a fraction of the galaxies will infall as part of groups, and often further action by the cluster might be necessary to fully explain the low star activity of observed cluster galaxies.

On the other hand, group environments may be much more relevant on the *morphological transformation* of galaxies, by hosting mergers between group members. As was realized early on, the high-velocity dispersion between galaxies in clusters makes cluster environments unsuitable for mergers to occur (Ostriker 1980; Mihos 2003; Fakhouri & Ma 2008; Fakhouri, Ma & Boylan-Kolchin 2010). However, observational evidence of mergers in clusters does exist (e.g. Moss 2006). For instance, the presence of shell dwarf galaxies in the outskirts of Virgo (Paudel et al. 2017; Zhang et al. 2020) is a vivid reminder that mergers can occur in galaxy clusters.

Mergers have been postulated as a viable mechanism to transform morphology, in particular in galaxy types that are commonly found in galaxy clusters, such as lenticular (S0) galaxies (Bekki 1998; D'Onofrio, Marziani & Buson 2015; Eliche-Moral et al. 2018) or blue compact dwarfs (BCDs; Bekki 2008; Zhang et al. 2020). Groups of galaxies infalling together will have shallower gravitational potentials than the cluster, allowing for lower velocity interactions to occur and, eventually, mergers (see e.g. Knebe et al. 2006; Vijayaraghavan & Ricker 2013; Bahé et al. 2019). Therefore, understanding the number of groups expected, their mass distribution and typical time-scales for group disruption are deemed essential to understand the possible contribution of mergers to the formation of, for instance, S0 and BCD galaxies while evaluating the need and contribution from additional secular and environmental formation channels for these morphologies.

In this paper, we use the Illustris simulations to address the impact of group infall in the assembly of Virgo-like galaxy clusters. We introduce our sample and definitions in Section 2. We characterize the fraction of galaxies in groups in Section 3, the dynamical time-scales for group disruption in Section 4, and the presence of mergers in Section 5. We summarize our main findings in Section 6.

2 NUMERICAL SIMULATIONS

We use the Illustris simulations (Vogelsberger et al. 2014a, b), a set of cosmological hydrodynamical numerical simulations run with the AREPO code (Springel 2010). The Illustris suite consists of a 106 Mpc on-a-side box simulated, in its highest resolution, with 1820^3 dark matter particles and an initially equal number of gas cells (Illustris-1). The corresponding mass per particle is $m_{\rm dm} = 6.3 \times 10^6$ M$_\odot$ for the dark matter and $m_{\rm gas} = 1.3 \times 10^6$ M$_\odot$ for the

baryonic component. The gravitational softening is $\epsilon \sim 0.7$ kpc, although the hydrodynamics can reach a higher spatial resolution in the high-density regions.

Illustris is evolved from initial conditions at redshift $z = 127$ forwards in time until $z = 0$ with cosmological parameters chosen to be consistent with results from Wilkinson Microwave Anisotropy Probe WMAP9 (Hinshaw et al. 2013). The main astrophysical processes shaping galaxy formation are included, such as the effects of cooling and heating of the gas, star formation, stellar and metallicity evolution, and feedback from stars as well as black hole sources. Detailed descriptions of the model can be found in previous papers: Vogelsberger et al. (2013, 2014b), Genel et al. (2014), Sijacki et al. (2015), and Nelson et al. (2015).

Structures are identified in a two-step process run on the fly with the simulation. First, groups are identified using the Friends-of-Friends algorithm, FoF (Davis et al. 1985) based solely on the spatial distribution of particles. Subsequently, SUBFIND is run using 6D information to identify galaxies and subhaloes that are self-bound structures within those groups (Springel et al. 2001; Dolag et al. 2009). Galaxies at the centre of the gravitational potential in each group are flagged as 'centrals', whereas all the remaining substructures identified in each group are flagged as 'satellites'. We use the SUBLINK trees to follow the temporal evolution of identified galaxies (Rodriguez-Gomez et al. 2015).

In this paper, we select the 10 most massive haloes in the Illustris-1 box at $z = 0$, corresponding to galaxy clusters with virial mass $M_{200} \sim 10^{14}\,\mathrm{M}_\odot$ [exact range $14.02 < \log(M_{200}/\mathrm{M}_\odot) < 14.37$]. We define virial quantities based on an overdensity contrast equal to 200 times the critical density of the Universe. The virial radius of our clusters is in the $0.97 < \log(r_{200}/\mathrm{Mpc}) < 1.26$ range with typical velocity dispersion within those radii $899 < \sigma_{200}/\mathrm{km\,s^{-1}} < 1073$. Within these 10 host haloes, we follow the evolution of all galaxies with stellar mass $M_\star \geq 1.5 \times 10^8\,\mathrm{M}_\odot$, corresponding to an average of ∼120 stellar particles in the lowest mass objects. Galaxy quantities such as stellar mass, $M_\star$, and gas mass, $M_{\rm gas}$, are measured within twice the half-mass radius of the stars (using `SubhaloMassInRadType` in the SUBFIND catalogues), while dark matter mass is defined as all dark matter particles gravitationally bound to a given subhalo (using the field `SubhaloMassType`).

2.1 Galaxy clusters and group infall

We show in Fig. 1 a stellar projection of our most massive galaxy cluster (FoF0), at present day, where the magenta large circle indicates the virial radius for this object. A total of 232 galaxies with $M_\star \geq 1.5 \times 10^8\,\mathrm{M}_\odot$ are identified within r_{200} in FoF0 at $z = 0$, which are visible here as substructure in the grey-scale map. The SUBLINK merger trees allow us to trace backwards on time the evolution of each galaxy until their time of infall, $t_{\rm inf}$, defined here as the previous snapshot when they join the same FoF group of the cluster progenitor. This definition typically places infalling galaxies at a distance of 2–3 times the virial radius of the cluster. It has been shown that environmental effects such as halo stripping start well beyond the virial radius (e.g. Behroozi et al. 2014) and peak at around $\sim 2r_{200}$, providing support for our $t_{\rm inf}$ definition.

We consider infalling 'galaxy groups' as any FoF group with at least two (but up to 80) galaxy members above our resolution cut on $M_\star$. Galaxies are classified as 'centrals' if they were the central object of their own FoF group at $t_{\rm inf}$, or as 'satellites' otherwise. With this definition, a galaxy will be considered accreted as a satellite even if they were outside the virial radius of their infalling group (although we briefly discuss the consequences of assuming more strict criteria in Section 3).

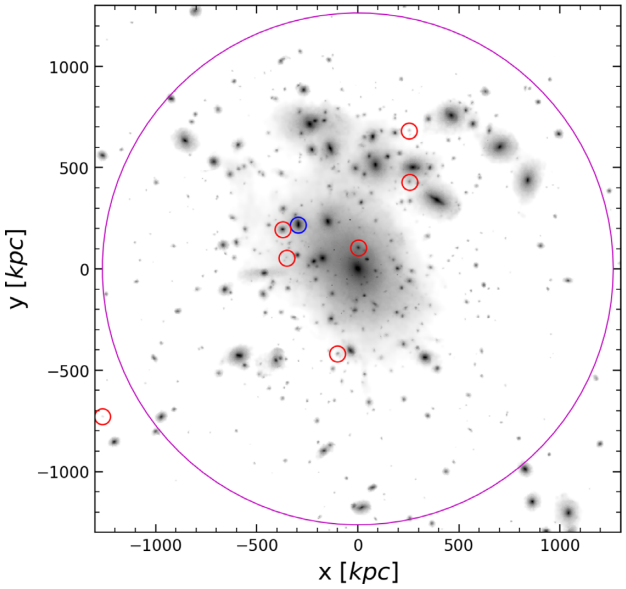

Figure 1. Projected stellar map at redshift $z = 0$ of the most massive cluster in our Illustris sample (FoF0). This object has a virial mass $M_{200} = 2.32 \times 10^{14}\,\mathrm{M}_\odot$ and 232 satellite galaxies with $\mathrm{M}_\star \geq 1.5 \times 10^8\,\mathrm{M}_\odot$ inside the virial radius $r_{200} = 1.27$ Mpc, indicated by the magenta circle. We highlight with small colour symbols a set of galaxies that were part of a group before joining the cluster at $z = 1.67$. The blue circle shows to central of the group and the red circles its surviving satellites. Despite their common origin, little evidence of the past association for these galaxies remains at present day.

From this point of view, our results characterize well the infall of loose associations of galaxies rather than fully virialized structures. After infall, tidal forces in the cluster will tend to dissolve these associations over time. For example, Fig. 1 highlights with red and blue circles all galaxies of a once single group, whose members lay today at $z = 0$ quite mixed within the cluster. Red indicates those galaxies accreted as satellites of this group, while blue corresponds to the central of the group. The virial mass of this substructure at infall is $M_{200}(t_{\rm inf}) = M_{200}^{\rm inf} = 4.69 \times 10^{12}\,\mathrm{M}_\odot$ and the stellar masses for the associated galaxies at infall are in the $\log(M_\star/\mathrm{M}_\odot) = [8.33 - 11]$ range.

The orbital evolution with time of these group members is shown in detail in Fig. 2. The left-hand panel shows the distance versus time for each galaxy in the group with respect to the cluster centre and emphasizes an initial coherence during the infall that is later weakened over time. This is particularly true after the first pericentre passage around $t \sim 7$ Gyr. Interestingly, some group members may gain energy due to several-body interactions, resulting in the display of odd orbits that place them today outside the virial radius of the cluster (dashed curve in Fig. 2, bottom left red circle in Fig. 1). These unorthodox orbits have been found in the literature to be common in simulations of group infall (e.g. Balogh, Navarro & Morris 2000; Sales et al. 2007; Ludlow et al. 2009) and related to the 'backsplash' radius region in observations and simulations (Pimbblet 2011; Muriel & Coenda 2014; Diemer et al. 2017).

The right-hand panel in Fig. 2 shows an XY projection of these orbits, and illustrates the disruption of the group over time as the satellite companions deviate from the trajectory of the central in

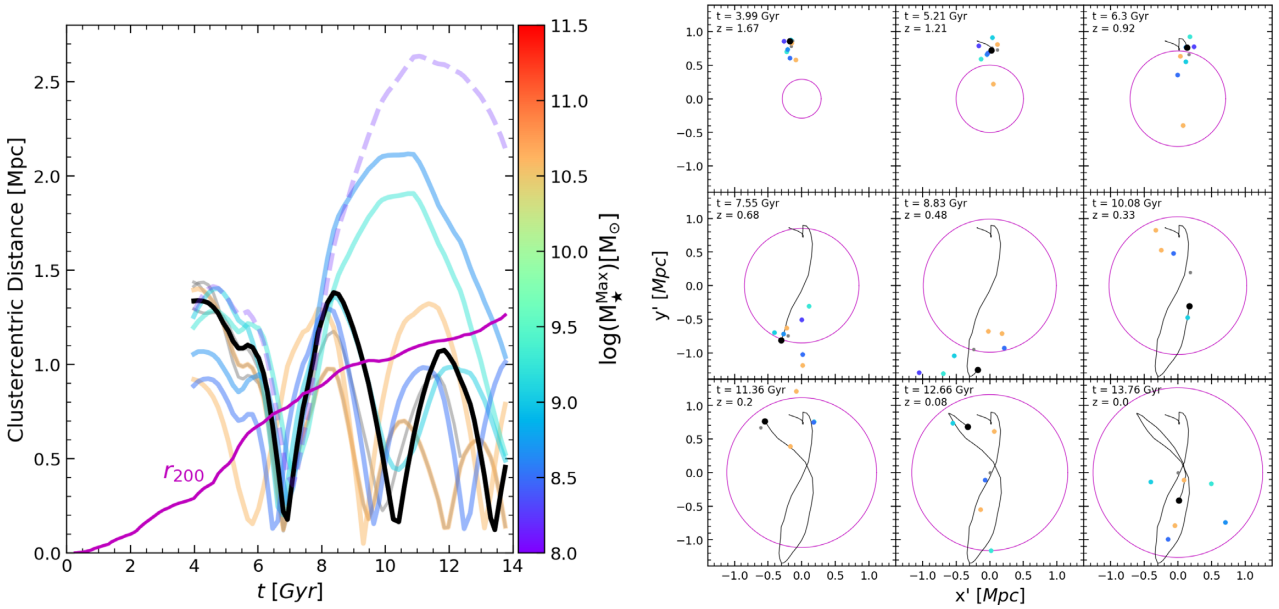

Figure 2. *Left:* orbit versus time for the infalling group of galaxies highlighted in Fig. 1 after their infall into FoF0. The central galaxy in the group is shown in black, and the satellites are colour coded according to their maximum stellar mass (see bar on the right). Note the propelling of three 'escapees' after the first pericentre passage, that takes them well beyond the virial radius of the host cluster (magenta curve). At $z = 0$, there is little coherence left among these orbits. *Right:* XY projections of the group at different times (see legends) with the trajectory of the central galaxy outlined with the thin black curve. The system has been rotated according to the angular momentum of the orbit of the central galaxy (pointing in the z-direction) and the colours are the same as in left-hand panel. Although the group starts very spatially clustered, the signal is appreciably weakened after the first and second pericentre within the cluster.

the group (thin black line). The combination of different assembly histories for each of the clusters combined with the time-scales over which these tidal disruptions of galaxy groups occur will determine the level of substructure – in both, position and velocities – that is expected in clusters within ΛCDM. In what follows, we study statistically the infall of galaxy groups on to our 10 simulated clusters and characterize their role in the assembly and dynamical evolution of their cluster hosts.

3 ACCRETION OF GALAXIES IN GROUPS

We start by validating the stellar mass function of our Illustris simulated galaxy clusters with observational constraints of Virgo and Fornax clusters [estimated virial masses: $M_{200} = 7.0 \pm 0.4 \times 10^{14}\,M_\odot$ and $M_{200} = 7 \pm 2 \times 10^{13}\,M_\odot$, respectively (Drinkwater, Gregg & Colless 2001; Karachentsev et al. 2014)]. Our clusters contain between 92 and 232 galaxies with $M_\star \geq 1.5 \times 10^8\,M_\odot$ that are today within r_{200}. Fig. 3 shows the (cumulative) stellar mass function of galaxies in each simulated cluster (solid colour lines). The scatter mostly corresponds to the range of virial masses selected and the different assembly histories sampled in the simulation. The numbers and distribution of $M_\star$ in our objects seem bracketed by measurements in Virgo (black triangle symbols, Rines & Geller 2008) and Fornax (black square symbols, Sarzi et al. 2018). Simulations also agree well with estimates from groups and clusters in SDSS (Yang et al. 2009) using the set of fitting parameters corresponding to the $\log(M_{200}/M_\odot) = [13.85 - 14.39]$ range that best approximates our systems.

The merger trees allow us to measure the fraction of the simulated galaxies that fell into their clusters as satellites of a galaxy group. We show this in the bottom panel of Fig. 3, where the colours correspond to the same individual clusters as the main panel and the black thicker solid line indicates the median of all clusters combined.

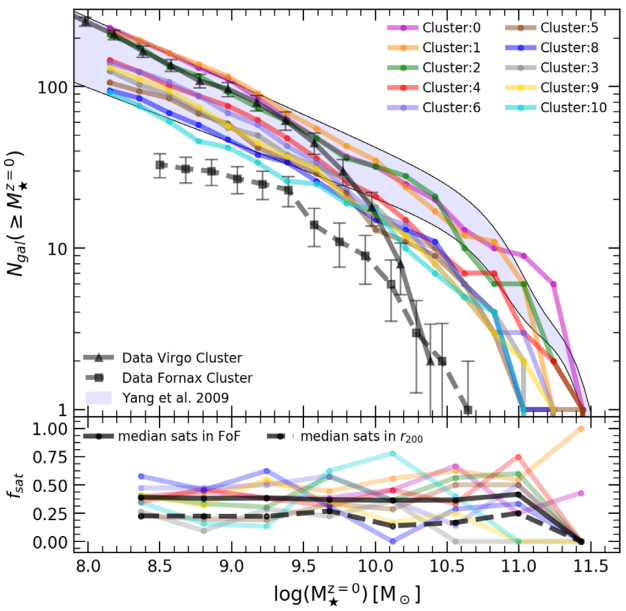

Figure 3. Cumulative galaxy stellar mass function at $z = 0$ for our 10 simulated clusters (colour lines). The predicted number of satellites at $z = 0$ in Illustris is in good agreement with observational data in similar mass ranges: the Virgo cluster (within ∼1 Mpc from M87 in solid grey, Rines & Geller 2008), Fornax (inside ∼0.7 Mpc in dashed grey, Sarzi et al. 2018), and in shaded blue SDSS groups and clusters [range $\log(M_h/M_\odot) \in (13.8, 14.4)$ in Yang et al. 2009]. The lower panel quantifies the fraction of these galaxies in each $M_\star$ bin that entered the clusters as satellites of groups with $N_{\rm gal} \geq 2$ members. We find a median of 38 per cent entered as satellites with little dependence on stellar mass (solid black curve), although variations from cluster to cluster are large (coloured lines). The dashed black line shows the median $f_{\rm sat}$ in the case of a more strict definition of satellite infall (see text for more details).

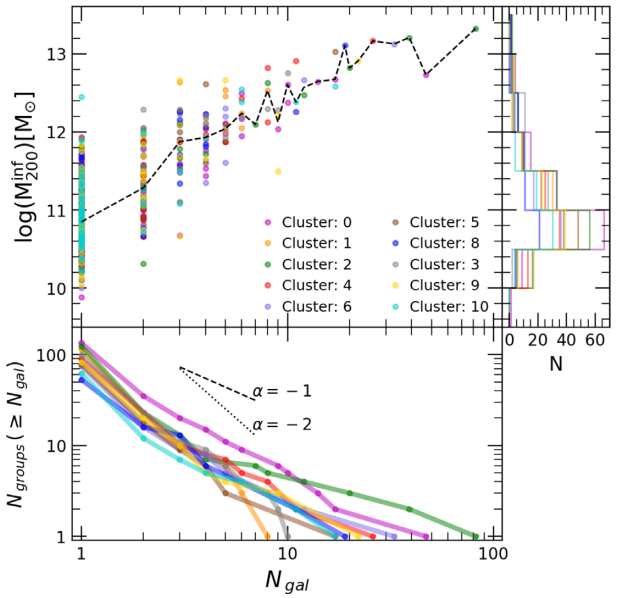

Figure 4. Multiplicity of infalling galaxy groups as a function of their virial mass. Multiplicity is defined as the number of galaxies, $N_{\rm gal}$, above our cut-off mass $M_\star \geq 1.5 \times 10^8\,M_\odot$ that enter as part of the same group. Low-mass groups will typically bring only one galaxy, but groups with masses $M^{\rm inf}_{200} \geq 2 \times 10^{12}\,M_\odot$ may contribute ∼10–80 galaxies. The bottom panel shows the cumulative multiplicity function (how many groups with $N_{\rm gal}$ larger than x) for each of our clusters. The histogram on the right shows how many objects of a given $M^{\rm inf}_{200}$ are found per cluster.

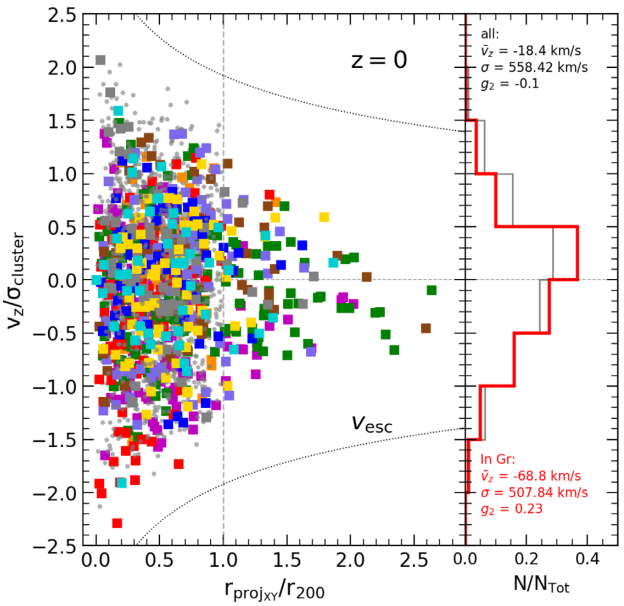

Figure 5. Projected distance versus line-of-sight velocity for galaxies in clusters at z = 0 (grey) with colours highlighting objects accreted as part of groups with $N_{\rm gal} \geq 2$ (colour code is the same as in Fig. 3). All galaxies are confined within the average escape velocity of the clusters (dotted curve). The vertical histograms on the right show that galaxies that infall in groups have a similar velocity distribution than normal galaxies when taken as a whole. Quoted values correspond to the mean, dispersion, and skewness of each distribution. Signatures of group infall, if present, dissolve quickly within the clusters.

A significant, although subdominant, fraction of galaxies enter the cluster as part of larger associations, with appreciable cluster-to-cluster scatter. Combining all our systems, we find that 38 ± 15 per cent of galaxies enter as satellites, with no clear dependence on galaxy stellar mass up to $M_\star \sim 10^{11}\,M_\odot$, after which the satellite fraction plummets to near zero. Dwarf galaxies with $M_\star \sim 10^8\,M_\odot$ are equally likely on average to be a satellite at infall as more massive galaxies in the $\sim L_\star$ range.

The exact values quoted above depend on the definition of what is considered a 'group' at infall. As mentioned in Section 2, we define as satellites all objects that are part of an FoF group. Note that other more strict definitions have been used in the literature before, for example, by requiring that satellites are within the virial radius of a bound group (e.g. Berrier et al. 2009; Choque-Challapa et al. 2019). For comparison, we find that when such criteria are used, our satellite fractions are about a factor of 2 smaller (22 ± 12 per cent) than with our default definition, see dashed line in bottom panel of Fig. 3. This is in excellent agreement with results reported in Berrier et al. (2009) for their $L_\star$ galaxies.

The break down of the accreted groups in mass and galaxy multiplicity is shown in Fig. 4. We use the virial mass at infall $M^{\rm inf}_{200}$ to quantify the masses of the FoF groups, which show, as expected, a clear correlation with the number of members in the group. In general, singletons and pairs are by far the more common accretion events (Choque-Challapa et al. 2019) for galaxies with $M_\star \geq 1.5 \times 10^8\,M_\odot$, but higher multiplicity is also common: about ∼10 groups with $N_{\rm gal} \geq 3$ galaxies are predicted during the assembly of Virgo-like clusters. (The quoted numbers correspond to the requirement that at least one member of the group will survive at $z = 0$.)

The variations from system to system are larger on the more numerous groups, where we expect a few (albeit likely) events brining ∼10 galaxies, with some extreme cases contributing up to 80 members (green curve, cluster 2). This scatter reflects the expected differences on the particular assembly history of each of the host clusters. The median virial mass for $N_{\rm gal} = 2$ accretions is $1.9 \times 10^{11}\,M_\odot$ suggesting that associations of dwarfs being accreted into clusters may be rather common. However, note the significant vertical scatter at $N_{\rm gal} = 2$, indicating that also MW-mass groups might bring in only one companion (besides the central) as a result of the large halo to halo variations.

4 DYNAMICAL EVOLUTION OF ACCRETED GROUPS

Despite the prevalence of group accretion shown in Section 3, evidence of substructure within clusters at $z = 0$ is not abundant, at least in phase space. Fig. 5 shows for our simulated clusters the velocity versus clustercentric distance of galaxies at present day, projected along a random line of sight to facilitate comparison to observations. Gray dots indicate galaxies that have fallen in as single objects, while colours indicate those aggregated as part of groups with $N_{\rm gal} \geq 2$ members. Dotted line shows the expected escape velocity assuming an NFW profile (Navarro et al. 1996) and concentration $c = 5.24$ following Duffy et al. (2008) for a $M_{200} = 1.6 \times 10^{14}\,M_\odot$ halo. The histograms shown in the right subpanel suggest that the global distribution of these two populations is not sufficiently different at $z = 0$ to distinguish substructure infall in this space. We have explicitly checked that this holds true also in a cluster-by-cluster basis.

Observationally, asymmetries in projected phase-space coordinates have been attributed to the accretion of substructure. For example, the Virgo cluster, where dwarf galaxies with r-band absolute

magnitude $-17 \geq M_r \geq -18$ show hints of an unrelaxed state, has been proposed as the smoking gun evidence for substructure infall (e.g. Lisker et al. 2018). Such strong signature is not present in our simulations despite the important role of group infall in our systems. Here, we have explicitly checked that the velocity distributions remain similar even when taking only low-mass galaxies ($M_\star \leq 10^9\,\mathrm{M}_\odot$ assuming $M_r = -17$ and mass-to-light ratio $\sim$1), as done in Virgo. One way to reconcile our theoretical expectations with the detection of substructure in observations is to assume that the clustering, either in position or velocities, of the infalling galaxy groups is rather quickly dissipated.

Qualitatively, a hint of this behaviour can be seen from the positions of galaxies in our example infalling group in Fig. 2, where the coherence in the orbital structure of the group is lost after the first pericentre at $t \sim 7$ Gyr. As a consequence, the distance between the galaxy members increases substantially, losing the clustering signature expected for substructures. This group dispersal effect even includes galaxies going back outside of the virial radius of the cluster at $z = 0$ while the rest of the group distributes within r_{200}. Naturally, a weakening of the correlation in velocities between galaxy members is also expected.

The stretching in space due to the tidal disruption of groups by the clusters can be measured by tracking the evolution of a characteristic size for each galaxy association after infall. We define σ_r as the rms dispersion of distances of all galaxies in each group, where $\sigma_r = \sqrt{\sigma_x^2 + \sigma_y^2 + \sigma_z^2}$, with $\sigma_x = \sqrt{\langle x_i^2\rangle - \langle x_i\rangle^2}$ and the same for σ_y and σ_z. More specifically, to quantify the time-scales involved in group disruption, we measure the time τ_d that it takes for a given group to double its size σ_r compared to that they had at infall time. We have explicitly checked that using other metrics to quantify size evolution give quantitative similar results as using σ_r (see Fig. A1 in Appendix for a discussion).

We show in Fig. 6 this 'disruption' time-scale τ_d as a function of the virial infall mass of our groups. Two points are worth highlighting. First, the size transformation occurs over short time-scales, $\tau_\mathrm{d} \sim$ 1–3 Gyr, albeit with significant scatter. This means that, if substructure is identified in observations of galaxies within clusters, it is likely associated with a relatively recent accretion event (see also Choque-Challapa et al. 2019, for similar conclusions). However, the scatter also allows for less common cases where the spatial clustering may last over longer time periods ($\sim$4–5 Gyr).

Secondly, we find a weak trend with mass: low-mass groups will double their spatial extend in about $\sim$1 Gyr after infall, while more massive groups take on average $\tau_\mathrm{d} \sim 3$ Gyr. These results can be interpreted as low-mass groups being less resilient to the tides from the central cluster, while the self-gravity of more massive groups allows them to remain bound for longer times after infall. The median trend is well fit by a relation: $\tau_\mathrm{d} = \alpha \log(\mathrm{M}^\mathrm{inf}_{200}/\mathrm{M}_\odot) + \beta$, with $\alpha = 0.8 \pm 0.1$ and $\beta = -7.6 \pm 1.5$, where uncertainties correspond to standard regression errors. However, there is a large scatter in this relation that might reflect the different accretion times and orbits of groups with similar $\mathrm{M}^\mathrm{inf}_{200}$.

Besides the spatial distribution of the group, the internal velocities of galaxy members are also changed by the dynamical evolution within the cluster. Following our definition of σ_r, we define σ_v as the velocity dispersion between galaxies in the same group. Fig. 7 shows σ_r versus σ_v for groups at infall (blue triangles) compared to the same groups at $z = 0$ (red circles). There is a clear evolution in both, size and velocity after infall. The median size of groups increases from $\log(\sigma_\mathrm{r}) \sim 1.99$ at infall to $\sim$2.63 at $z = 0$, corresponding to $\sim\times$4.4 average increase in size at present day. The velocity dispersion between galaxy members also increases by a factor $\sim\times$2.5 in the same time period (with medians $\log(\sigma_\mathrm{v}) \sim 2.27$ at infall compared to $\sim$2.67 at present day). Groups get less spatially clustered and increase their velocity dispersion with time.

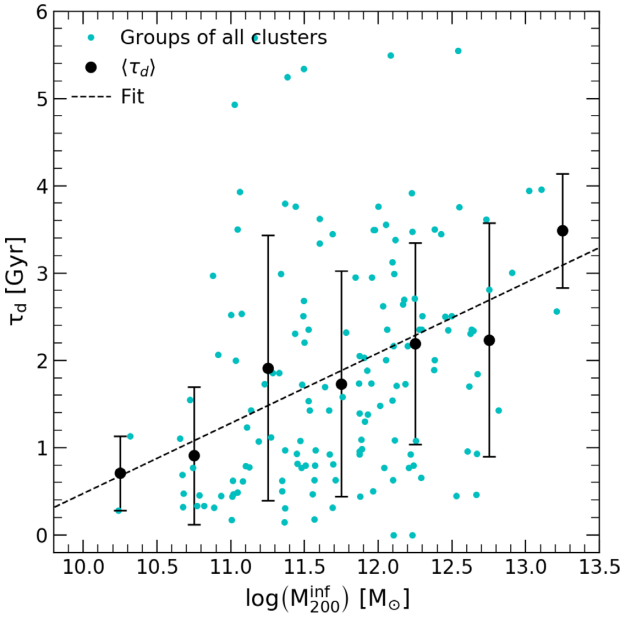

Figure 6. Time τ_d that is needed for each group to double their radial size, σ_r, as a function of the infall mass of the group. Individual groups identified in the 10 simulated clusters are shown in cyan circles with the median τ_d in M^inf_{200} bins shown in black symbols and bars for the standard deviation. There is a very weak dependence with the mass of the form: $\tau_\mathrm{d} = \alpha \log(\mathrm{M}^\mathrm{inf}_{200}/\mathrm{M}_\odot) + \beta$, with $\alpha = 0.8 \pm 0.1$ and $\beta = -7.6 \pm 1.5$ (dashed line), but the trend is greatly superseded by the large scatter at each group mass. The large dispersion is attributed to the different orbits, infall times, and number of members in each group.

How large and how hot these groups become at $z = 0$? Naively, one would expect that the size of the cluster and its velocity dispersion are natural boundaries to these quantities. We show in Fig. 7 (green square) the average size (virial radius) and the average velocity dispersion of our clusters. Additionally, for better reference, we also show the median σ_r and σ_v that one would measure by taking random groups of N = 2, 3, 5, and 20 galaxies in our clusters that did not infall as part of a group (filled black circles are the median of 100 random samplings). By construction, these filled circles represent the expected closest-to-virialized σ_r and σ_v in these clusters and demonstrate that $\gtrsim$5 members should be expected to trace average sizes and velocity dispersions in the cluster if properly relaxed.

Instead, we find that galaxies that fell in as part of groups are today at $z = 0$ typically below the velocity of these random samples (red symbols), suggesting that although the dynamical evolution in the cluster tends to erase the dynamical identity of substructures, groups that have fallen in remain kinematically colder than the surrounding cluster. The same is not exactly true for the spatial distribution of groups, which may even exceed the virial radius of the cluster (red points to the right of the dotted green vertical line). This is the case for some groups where galaxy members were ejected outside r_{200}, as the group showcased in Fig. 2. The median σ_r of galaxies in groups is still more clustered that the random samples (see vertical dashed red line), but the effect in position is less systematic than in velocity.

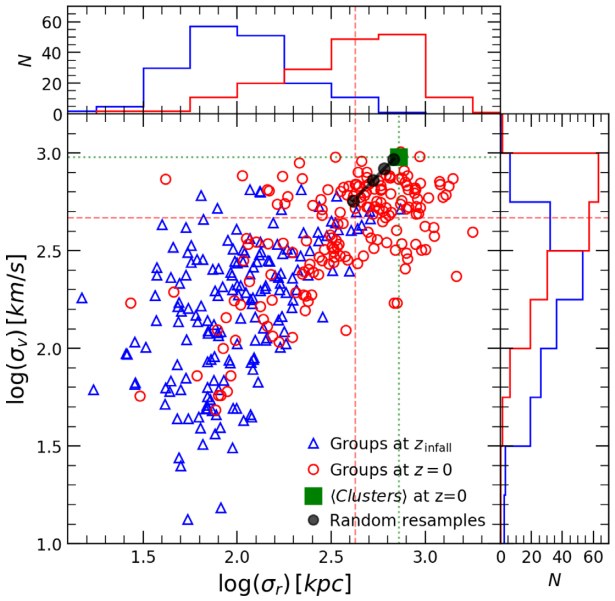

Figure 7. Time evolution of groups in characteristic size, σ_r, versus their typical velocity dispersion, σ_v. Values at infall for each group are shown in blue while $z = 0$ are shown in red. Groups after infall tend to thermalize with the state of the cluster, systematically increasing their sizes and velocities (see blue versus red histograms along each axis). However, despite of the dynamical heating, groups tend to remain colder and more compact than the host cluster itself (compare the median of groups in dashed red lines with the median virial cluster values shown by thin dotted green lines and filled green square). The filled black circle symbols connected by a continuous line show the average σ_r and σ_v of 100 realizations with N = 2, 3, 5, and 20 randomly selected galaxies in the simulated clusters that are *not* accreted as part of groups. The distribution of red symbols (group infallers) is clearly shifted towards lower σ_r and σ_v than these random samples, confirming that group infall provides a special kinematical environment for members compared to the rest of the relaxed cluster population.

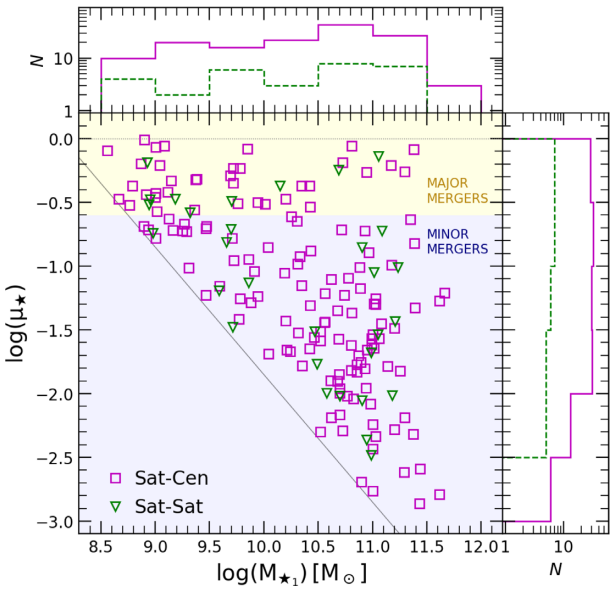

Figure 8. Stellar mass ratio $\mu_\star$ of the 171 identified mergers in and around clusters as a function of the stellar mass of the most massive companion pre-merger $M_{\star_1}$. All mergers found are hosted by groups that fell into the cluster, either between a satellite galaxy and the central of the group (Sat–Cen, magenta squares) or between two satellites in the group (Sat–Sat, green triangles). We adopt the mass ratio $\mu_\star = 0.25$ to distinguish between major (yellow) and minor (purple) mergers following Rodriguez-Gomez et al. (2015). A significant fraction (26.3 per cent) of the mergers occurring in clusters are major according to this definition.

5 MERGERS OF GALAXIES IN GROUPS

The lower velocities between galaxies associated with the infalling groups found in Fig. 7 may play a vital role in facilitating the conditions for mergers to occur within (or in the outskirts) of massive clusters. This is perhaps important to help explain the observational evidence for young mergers in nearby galaxy clusters like Virgo (e.g. Zhang et al. 2020). We follow the assembly of our 10 clusters in Illustris and identify possible merger events, their mass ratios, times and location with respect to the cluster centre.

We find a large number of galaxies that merge to the central galaxy in the cluster, referred to as 'brightest cluster galaxy', or BCG. These mergers build the stellar mass of the BCG as well as the intracluster light component and are not the main focus of this paper (see for instance Rodriguez-Gomez et al. 2015, for a quantification of accreted component in BCGs). Instead, we identify mergers that occur near or within the clusters, and that involve only satellite galaxies in the clusters. We find an average of $\sim 17 \pm 9$ mergers per cluster above our resolution limits, where the quoted uncertainty corresponds to the rms of our clusters sample.

This confirms that indeed mergers can occur in cluster environments despite the high velocity of galaxies in such environment. Most importantly, *all mergers identified occur in galaxies that fell into the clusters as part of groups with $N \geq 2$ members*. In other words, mergers in clusters do not occur among galaxies that infall as singletons, in agreement with expectations based on the typical high velocity in clusters (Ostriker 1980).

Fig. 8 shows the stellar mass ratios $\mu_\star = M_{\star_2}/M_{\star_1}$ of all mergers detected, where the stellar mass of the most massive galaxy involved is defined as $M_{\star_1}$ and the secondary is $M_{\star_2}$. We follow the convention introduced in Rodriguez-Gomez et al. (2015) and record both masses at the time when the secondary has its maximum mass, to avoid artificial lowering of the mass ratio due to subsequent stripping before the merger (see Rodriguez-Gomez et al. 2015, for a detailed discussion).

We further divide the mergers in Fig. 8 into two kinds: those between a satellite and the central of the group (Sat–Cen, magenta squares), and those involving two satellites within a group where neither is the central (Sat–Sat, green triangles). The distributions do not differ substantially, except that mergers with the centrals of the groups are more likely (82 per cent).

Following Rodriguez-Gomez et al. (2015), we consider galaxy mergers with stellar mass ratio $\mu_\star \gtrsim 0.25$ as major mergers. As expected from numerical limitations, we can only follow major mergers in our dwarf galaxies regime ($M_\star \leq 10^9\,M_\odot$) while for $M_\star \geq 10^{10.5}\,M_\odot$, we resolve well into the minor mergers events. Sat–Sat and Sat–Cen show similar distributions for major and minor mergers (see vertical histogram on the right of Fig. 8).

Mergers may occur anywhere from the time of infall until today and they can therefore happen also in the immediately surrounding region of the clusters ($1 \leq r/r_{200} \leq 2$–3). We study the distribution of time and location of these mergers in Fig. 9, where symbols correspond to each of the Sat–Sat and Sat–Cen merger identified and colours indicate mass ratio $\mu_\star = M_{\star_2}/M_{\star_1}$ using the colour coding shown in the vertical bar. Although the majority of these mergers happen within the group environment before crossing the virial

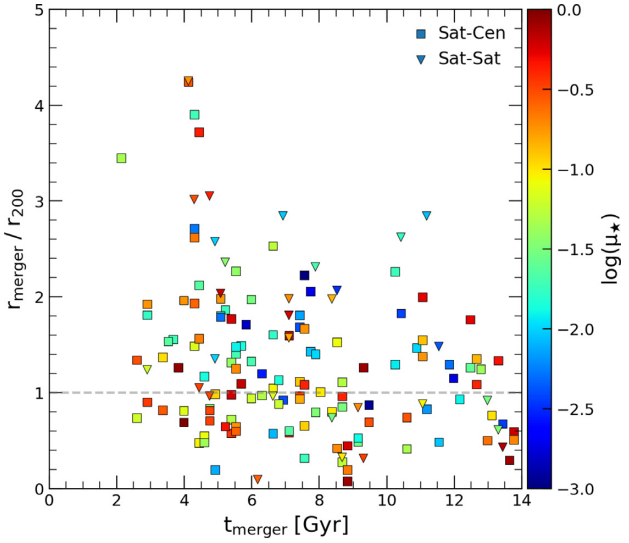

Figure 9. Distance (from the centre of the clusters) versus time where the mergers occur. Symbols are colour coded by stellar mass ratio $\mu_\star$ (see colour bar). The grey horizontal line indicates $r = r_{200}$. Around ∼40 per cent of the mergers occur inside the virial radii of the clusters with no significant correlation with time or mass ratio.

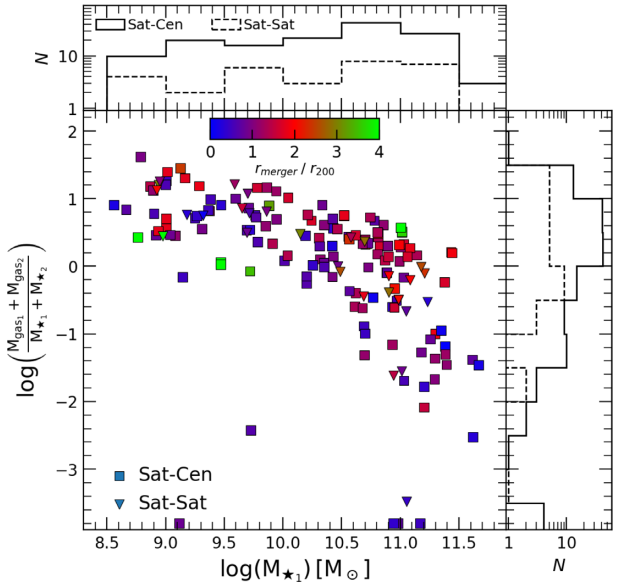

Figure 10. Gas fraction $f_{gas} = M_{gas}/M_\star$ in mergers in and around clusters as a function of the stellar mass of the primary galaxy $M_{\star_1}$. Triangle/squares are used for Sat–Sat and Sat–Cen mergers, colour coded according to the location of the merger (see colour bar). Histograms show the distribution along each axis for Sat–Sat and Sat–Cen events. Mergers are gas rich for the dwarfs domain, but transition into a mix of gas rich and gas poor for more massive galaxies. These mergers may provide a natural avenue for the formation of S0s and BCD galaxies in galaxy clusters.

radius, still a significant fraction of mergers, ∼40 per cent, happen within r_{200} (corresponding to an average number per cluster of 7 ± 3 throughout its evolution). Moreover, some of these even occur deep into the inner regions of the cluster host. The significant number of mergers within clusters is encouraging given the important role expected of mergers in the morphology of galaxies in high-density regions.

The final fate of these merger remnants will depend on the mass of the intervening galaxies and their gas content. On the dwarfs regime, mergers are the main mechanism thought to produce BCDs with both, observational data as well as idealized numerical simulations showing the feasibility of this formation path (e.g. Bekki 1998; Östlin et al. 2001). Such mergers will typically involve two dwarf galaxies with similar masses and should contain gas to fuel the central starburst that gives rise to the dense inner blue core. On the other hand, gas-free similar mass dwarf–dwarf mergers would explain better the presence of low surface brightness shells as found in a couple of dwarfs in deep studies of the outskirts of Virgo (Paudel et al. 2017; Zhang et al. 2020).

For more massive galaxies, mergers could be important contributors to the build up of the S0 (lenticular) population (Baugh, Cole & Frenk 1996; Somerville & Kolatt 1999; Bekki 2008; Hopkins et al. 2008; Arnold et al. 2011), with some discussion on the need of some gas to rebuild the disc (Naab, Jesseit & Burkert 2006) while other authors find suitable S0 remnants that form even in dry (gas-poor) mergers (Tapia et al. 2014; Eliche-Moral et al. 2018). However, these numerical simulations have mostly focused on idealized experiments, while the final number of S0-like galaxies expected in clusters from mergers will depend on the location and gas ratios of these mergers occurring within the cosmological set-up

We explore these scenarios in Fig. 10, where we show the gas fraction of the mergers in our clusters (which, as explained above occur all within the galaxy groups) as a function of the primary mass and colour coded by the position within the clusters where the merger occurred. Gas ratios are defined as $f_{gas} = M_{gas}/M_\star = \left(M_{gas_1} + M_{gas_2}\right) / \left(M_{\star_1} + M_{\star_2}\right)$. We find that for dwarf galaxies with $M_\star \leq 10^9$ M$_\odot$ mergers are in their majority gas rich, supporting this scenario as formation path for BCDs in groups and clusters.

Although several studies of BCDs exist in nearby clusters (e.g. Drinkwater et al. 1996; Vaduvescu et al. 2011; Zhao, Gao & Gu 2013; Meyer et al. 2014; Vaduvescu et al. 2014), very few cover the whole cluster area with completeness enough to quantify the frequency of BCDs compared to other kinds of dwarfs. The Virgo cluster given its relative proximity offers perhaps the best data. Based on photometric plates, Binggeli, Sandage & Tammann (1985) reported ∼38 BCDs (member) candidates with B-band magnitude $M_B \leq -13.09$. Of these, Meyer et al. (2014) studied 30 objects with $M_r \leq -14$ in detail confirming their BCDs nature and association to Virgo. Assuming a mass-to-light ratio of unity, this sample includes 12 dwarfs with $M_\star \geq 10^{8.2}$ M$_\odot$, the resolution limit of our study. We find 10 dwarf–dwarf gas-rich mergers that occur within $r < 2r_{200}$ in our 10 clusters sample (considering all galaxies with $M_\star \leq 10^9$ M$_\odot$). This suggests that at least some of these BCDs could be explained by dwarf–dwarf mergers while the majority may have already have fallen in as a BCD. However, more detailed comparisons should be made in the future that include other clusters once complete surveys of BCDs become available in the literature.

Interestingly, a few low-mass galaxies with $M_\star < 10^{10}$ M$_\odot$ experiencing dry mergers are also found ($f_{gas} < 0.1$) in our simulated sample, although they are rare. Whether these events would be enough to explain the observational findings of dwarfs with shell-like features is currently an open question since no complete samples exist of these objects with low surface brightness features. However, it is encouraging that within the limited resolution of these simulations a few cases arise that may compare well with these peculiar objects found in Virgo (e.g. Paudel et al. 2017; Zhang et al. 2020).

While most of the mergers in the low-mass end are predicted to be gas rich, for MW-like galaxies and above, we find a wider range

of possible gas fractions, in particular with most mergers being gas poor for $M_\star \geq 10^{10.5}\,\mathrm{M}_\odot$. There is a weak trend suggesting that gas-poor mergers occur preferentially within r_{200} of the cluster (blue and purple colours), perhaps highlighting the *combined* effects of group infall and cluster environment in removing the gas of $L_\star$ galaxies.[1]

We conclude with the remark that mergers can occur within and around galaxy clusters. They are hosted always within the more gentle environment of infalling groups that characterize the hierarchical assembly of clusters. However, we detect an average of 17 mergers per cluster accumulated during the entire evolution (but up to 42 for our most massive object, 15 of which occur within r_{200}). For reference, a cluster like Virgo has ∼49 S0s and another ∼30 dwarfs S0 galaxies (Binggeli et al. 1987; van den Bergh 2009).

This means that mergers, specially for $M_\star \geq 10^{10}\,\mathrm{M}_\odot$ and above, may have a moderate to significant contribution to the build up of S0s in clusters. However, depending on the particular assembly history and merger events registered in each cluster, it is likely that other mechanisms, for instance the gas removal by ram pressure (Gunn & Gott 1972) followed by secular effects, will contribute as well to explain the total sample of S0 galaxies today. This is in good agreement with recent observational results suggesting more than one mechanism, including mergers, lead to the formation of lenticular galaxies (Fraser-McKelvie et al. 2018; Coccato et al. 2020; Dolfi et al. 2020).

6 SUMMARY AND CONCLUSIONS

We use the Illustris cosmological hydrodynamical simulations to study the assembly of the 10 most massive galaxy clusters in the box, with typical virial masses $M_{200} \sim 10^{14}\,\mathrm{M}_\odot$. In particular, we address the contribution of group infall to the surviving population of galaxies, their cluster dynamics, and the occurrence of mergers nearby or within clusters. We follow the evolution of galaxies with $M_\star \geq 1.5 \times 10^8\,\mathrm{M}_\odot$, covering a wide range of galaxy masses, from dwarfs comparable to the SMC to the more massive $M_\star \sim 10^{11.5}\,\mathrm{M}_\odot$ galaxies in clusters. Our results can be summarized as follows.

(i) We find that 38 ± 15 per cent of present-day galaxies in clusters have fallen in as part of larger groups or galaxy associations, here defined as groups identified by the FoF algorithm. More strict satellite criteria – for example, requiring that galaxies are within the virial radius of an infalling group – lowers the result to ∼22 per cent of galaxies entering as satellites. This fraction is independent of galaxy stellar mass and shows large dispersion from cluster-to-cluster depending on the particular assembly history. Our results agree well with previous reports in the literature (e.g. Berrier et al. 2009) and extend the analysis to lower mass dwarfs and also to hydrodynamical simulations compared to *N*-body only runs.

(ii) Poor groups are common: galaxies that are not accreted as single objects will typically come with only one or two companions above our resolution limit. All our clusters accreted at least one group with 10 galaxies or more, reaching up to 80 galaxy members in our most extreme case.

(iii) These groups will quickly evolve in phase space after infall, making their detection in observations rather difficult. The timescale to double the size and the velocity dispersion of the group is in the range $\tau_\mathrm{d} \sim$ [0.2–5] Gyr, with only a modest dependence on group mass. Instead, different orbits and accretion times are likely to dominate the scatter.

(iv) Although groups become dynamically hotter under the tidal effects of the cluster, the relative velocity between the once group members remains lower than the average of random galaxies in the cluster. This correlated motion, allow for low-velocity encounters and, eventually, mergers to occur in the cluster and its surroundings. All identified mergers in our simulation occurred within galaxy groups, with no mergers registered between galaxies that infall as singletons (excluding those mergers with the BCG).

(v) Mergers in groups occur across the entire stellar mass range, from dwarfs to $L_\star$ galaxies. The location of these mergers varies, with ∼60 per cent occurring outside the clusters, at distances between 1–$4r_{200}$, and ∼40 per cent happening within the r_{200} of the clusters themselves. Our study offers solid support to the scenario where group infall promotes the occurrence of mergers even within the high-velocity dispersion environment of clusters.

(vi) The gas ratios of these mergers depend critically on galaxy mass: they are strongly gas rich dominated for $M_\star \leq 10^9\,\mathrm{M}_\odot$, while a combination of gas rich and gas poor is found for more massive galaxies with $M_\star \geq 10^{10}\,\mathrm{M}_\odot$.

Based on studies of idealized (non-cosmological) simulations showing that mergers may contribute to the formation of BCDs and S0 galaxies in clusters (Bekki 1998; Bournaud, Jog & Combes 2005; Bekki 2008; Eliche-Moral et al. 2018), we conclude that such mergers exist naturally within the ΛCDM scenario as part of the predicted group infall. The number of events can show large variations from cluster to cluster, but it suggests that mergers may contribute significantly to the build up of the morphological mix even in high-density environments.

We hasten to add that the observed population of S0s in clusters may be larger than the number of predicted mergers in ΛCDM, requiring of additional formation paths for S0 galaxies. These may include, for instance, secular evolution, gas removal/fading, or unstable high redshift discs (van den Bergh 2009; Eliche-Moral et al. 2013; Saha & Cortesi 2018) in good agreement with observational constraints. The different kinematical and structural properties of S0s created by these different mechanisms are still challenging to predict with sufficient numerical resolution for simulations in the cosmological context, but observational studies are starting to highlight promising paths to disentangle between the different formation scenarios proposed (see e.g. Fraser-McKelvie et al. 2018; Coccato et al. 2020).

Encouragingly, we identify at least two gas-free dwarf–dwarf mergers ($M_\star < 10^{10}\,\mathrm{M}_\odot$) in the outskirts of our clusters, which may help explain the discovery of shell-like low-surface brightness stellar features around dwarfs in Virgo. However, higher numerical resolution is needed in order to have more predictive power on the exact morphology of the remnants. Looking forward, efforts like TNG50 (Nelson et al. 2019; Pillepich et al. 2019) or RomulusC (Tremmel et al. 2019) simulations may offer promising new frontiers in our understanding of mergers in cluster environments and their role in the build up of the morphology of cluster galaxies.

ACKNOWLEDGEMENTS

The authors would like to thank the anonymous referee for a constructive and detailed report that helped improve the earlier version of this paper. JAB and MGA acknowledge financial support from CONICET through PIP 11220170100527CO grant. LVS

[1]Caution might be exercised, as this effect may be affected by the lower gas fractions predicted in groups in Illustris compared to observations, an issue later improved in the related TNG simulations (Pillepich et al. 2018).

is grateful for funding support from UC MEXUS, NASA-ATP-80NSSC20K0566, and NSF-CAREER-1945310 grants.

DATA AVAILABILITY

This paper is based on halo catalogues and merger trees from the Illustris Project (Vogelsberger et al. 2014a, b). These data are publicly available at https://www.illustris-project.org/. The catalogue of infalling groups, mergers, and other products of this analysis may be shared upon request to the corresponding author if no further conflict exists with ongoing projects.

REFERENCES

Arnold J. A., Romanowsky A. J., Brodie J. P., Chomiuk L., Spitler L. R., Strader J., Benson A. J., Forbes D. A., 2011, ApJ, 736, L26
Bahé Y. M. et al., 2019, MNRAS, 485, 2287
Balogh M. L., Navarro J. F., Morris S. L., 2000, ApJ, 540, 113
Baugh C. M., Cole S., Frenk C. S., 1996, MNRAS, 283, 1361
Behroozi P. S., Wechsler R. H., Lu Y., Hahn O., Busha M. T., Klypin A., Primack J. R., 2014, ApJ, 787, 156
Bekki K., 1998, ApJ, 502, L133
Bekki K., 2008, MNRAS, 388, L10
Berrier J. C., Stewart K. R., Bullock J. S., Purcell C. W., Barton E. J., Wechsler R. H., 2009, ApJ, 690, 1292
Binggeli B., Sandage A., Tammann G. A., 1985, AJ, 90, 1681
Binggeli B., Tammann G. A., Sandage A., 1987, AJ, 94, 251
Biviano A., Katgert P., Thomas T., Adami C., 2002, A&A, 387, 8
Bournaud F., Jog C. J., Combes F., 2005, A&A, 437, 69
Boylan-Kolchin M., Springel V., White S. D. M., Jenkins A., 2010, MNRAS, 406, 896
Busha M. T., Marshall P. J., Wechsler R. H., Klypin A., Primack J., 2011, ApJ, 743, 40
Choque-Challapa N., Smith R., Candlish G., Peletier R., Shin J., 2019, MNRAS, 490, 3654
Coccato L. et al., 2020, MNRAS, 492, 2955
Cohn J. D., 2012, MNRAS, 419, 1017
Conselice C. J., Gallagher J. S. I., 1998, MNRAS, 297, L34
D'Onghia E., 2008, preprint (arXiv:0802.0302)
D'Onofrio M., Marziani P., Buson L., 2015, Frontiers Astron. Space Sci., 2, 4
Davis M., Efstathiou G., Frenk C. S., White S. D. M., 1985, ApJ, 292, 371
De Lucia G., 2012, Astron. Nachr., 333, 460
De Lucia G., Weinmann S., Poggianti B. M., Aragón-Salamanca A., Zaritsky D., 2012, MNRAS, 423, 1277
Diemer B., Mansfield P., Kravtsov A. V., More S., 2017, ApJ, 843, 140
Dolag K., Borgani S., Murante G., Springel V., 2009, MNRAS, 399, 497
Dolfi A. et al., 2020, MNRAS, 495, 1321
Drinkwater M. J., Currie M. J., Young C. K., Hardy E., Yearsley J. M., 1996, MNRAS, 279, 595
Drinkwater M. J., Gregg M. D., Colless M., 2001, ApJ, 548, L139
Duffy A. R., Schaye J., Kay S. T., Dalla Vecchia C., 2008, MNRAS, 390, L64
Eliche-Moral M. C., González-García A. C., Aguerri J. A. L., Gallego J., Zamorano J., Balcells M., Prieto M., 2013, A&A, 552, A67
Eliche-Moral M. C., Rodríguez-Pérez C., Borlaff A., Querejeta M., Tapia T., 2018, A&A, 617, A113
Fakhouri O., Ma C.-P., 2008, MNRAS, 386, 577
Fakhouri O., Ma C.-P., Boylan-Kolchin M., 2010, MNRAS, 406, 2267
Ferrarese L. et al., 2020, ApJ, 890, 128
Fraser-McKelvie A., Aragón-Salamanca A., Merrifield M., Tabor M., Bernardi M., Drory N., Parikh T., Argudo-Fernández M., 2018, MNRAS, 481, 5580
Genel S. et al., 2014, MNRAS, 445, 175
Giocoli C., Tormen G., van den Bosch F. C., 2008, MNRAS, 386, 2135
Giocoli C., Tormen G., Sheth R. K., van den Bosch F. C., 2010, MNRAS, 404, 502
Gonzalez-Casado G., Mamon G. A., Salvador-Sole E., 1994, ApJ, 433, L61
Gunn J. E., Gott J. Richard I., 1972, ApJ, 176, 1
Gurzadyan V. G., Mazure A., 1998, MNRAS, 295, 177
Hinshaw G. et al., 2013, ApJS, 208, 19
Hopkins P. F., Cox T. J., Kereš D., Hernquist L., 2008, ApJS, 175, 390
Iodice E. et al., 2017, ApJ, 839, 21
Iodice E. et al., 2019, A&A, 627, A136
Jauzac M. et al., 2016, MNRAS, 463, 3876
Jethwa P., Erkal D., Belokurov V., 2016, MNRAS, 461, 2212
Kallivayalil N., van der Marel R. P., Alcock C., 2006, ApJ, 652, 1213
Kallivayalil N., van der Marel R. P., Besla G., Anderson J., Alcock C., 2013, ApJ, 764, 161
Karachentsev I. D., Tully R. B., Wu P.-F., Shaya E. J., Dolphin A. E., 2014, ApJ, 782, 4
Knebe A., Power C., Gill S. P. D., Gibson B. K., 2006, MNRAS, 368, 741
Lisker T., Vijayaraghavan R., Janz J., Gallagher John S. I., Engler C., Urich L., 2018, ApJ, 865, 40
Ludlow A. D., Navarro J. F., Springel V., Jenkins A., Frenk C. S., Helmi A., 2009, ApJ, 692, 931
McGee S. L., Balogh M. L., Bower R. G., Font A. S., McCarthy I. G., 2009, MNRAS, 400, 937
Meyer H. T., Lisker T., Janz J., Papaderos P., 2014, A&A, 562, A49
Mihos C., 2003, preprint (astro-ph/0305512)
Moss C., 2006, MNRAS, 373, 167
Muriel H., Coenda V., 2014, A&A, 564, A85
Naab T., Jesseit R., Burkert A., 2006, MNRAS, 372, 839
Natarajan P., Kneib J.-P., Smail I., Treu T., Ellis R., Moran S., Limousin M., Czoske O., 2009, ApJ, 693, 970
Navarro J. F., Frenk C. S., White S. D. M., 1996, ApJ, 462, 563
Navarro J. F., Frenk C. S., White S. D. M., 1997, ApJ, 490, 493
Nelson D. et al., 2015, Astron. Comput., 13, 12
Nelson D. et al., 2019, MNRAS, 490, 3234
Östlin G., Amram P., Bergvall N., Masegosa J., Boulesteix J., Márquez I., 2001, A&A, 374, 800
Ostriker J. P., 1980, Comments Astrophys., 8, 177
Owers M. S., Couch W. J., Nulsen P. E. J., 2009a, ApJ, 693, 901
Owers M. S., Nulsen P. E. J., Couch W. J., Markevitch M., 2009b, ApJ, 704, 1349
Paudel S. et al., 2017, ApJ, 834, 66
Pillepich A. et al., 2018, MNRAS, 473, 4077
Pillepich A. et al., 2019, MNRAS, 490, 3196
Pimbblet K. A., 2011, MNRAS, 411, 2637
Rines K., Geller M. J., 2008, AJ, 135, 1837
Roberts I. D., Parker L. C., 2017, MNRAS, 467, 3268
Rodriguez-Gomez V. et al., 2015, MNRAS, 449, 49
Román J., Trujillo I., 2017, MNRAS, 468, 4039
Saha K., Cortesi A., 2018, ApJ, 862, L12
Sales L. V., Navarro J. F., Abadi M. G., Steinmetz M., 2007, MNRAS, 379, 1464
Sales L. V., Navarro J. F., Cooper A. P., White S. D. M., Frenk C. S., Helmi A., 2011, MNRAS, 418, 648
Sales L. V., Navarro J. F., Kallivayalil N., Frenk C. S., 2017, MNRAS, 465, 1879
Sarron F., Adami C., Durret F., Laigle C., 2019, A&A, 632, A49
Sarzi M. et al., 2018, A&A, 616, A121
Sijacki D., Vogelsberger M., Genel S., Springel V., Torrey P., Snyder G. F., Nelson D., Hernquist L., 2015, MNRAS, 452, 575
Somerville R. S., Kolatt T. S., 1999, MNRAS, 305, 1
Springel V., 2010, MNRAS, 401, 791
Springel V., White S. D. M., Tormen G., Kauffmann G., 2001, MNRAS, 328, 726
Su Y. et al., 2019, AJ, 158, 6
Tapia T. et al., 2014, A&A, 565, A31
Taylor J. E., Babul A., 2004, MNRAS, 348, 811
Taylor J. E., Babul A., 2005a, MNRAS, 364, 515
Taylor J. E., Babul A., 2005b, MNRAS, 364, 535

Tremmel M. et al., 2019, MNRAS, 483, 3336
Trentham N., Hodgkin S., 2002, MNRAS, 333, 423
Treu T., Ellis R. S., Kneib J.-P., Dressler A., Smail I., Czoske O., Oemler A., Natarajan P., 2003, ApJ, 591, 53
Vaduvescu O., Kehrig C., Vilchez J. M., Unda-Sanzana E., 2011, A&A, 533, A65
Vaduvescu O., Kehrig C., Bassino L. P., Smith Castelli A. V., Calderón J. P., 2014, A&A, 563, A118
van den Bergh S., 2009, ApJ, 702, 1502
van den Bosch F. C., Tormen G., Giocoli C., 2005, MNRAS, 359, 1029
Venhola A. et al., 2017, A&A, 608, A142
Vijayaraghavan R., Ricker P. M., 2013, MNRAS, 435, 2713
Vijayaraghavan R., Gallagher J. S., Ricker P. M., 2015, MNRAS, 447, 3623
Vogelsberger M., Genel S., Sijacki D., Torrey P., Springel V., Hernquist L., 2013, MNRAS, 436, 3031
Vogelsberger M. et al., 2014a, MNRAS, 444, 1518
Vogelsberger M. et al., 2014b, Nature, 509, 177
Yang X., Mo H. J., van den Bosch F. C., 2009, ApJ, 695, 900
Yang X., Mo H. J., Zhang Y., van den Bosch F. C., 2011, ApJ, 741, 13
Zhang Y.-Y., Reiprich T. H., Finoguenov A., Hudson D. S., Sarazin C. L., 2009, ApJ, 699, 1178
Zhang H.-X. et al., 2020, ApJ, 891, L23
Zhao Y., Gao Y., Gu Q., 2013, ApJ, 764, 44

APPENDIX A: MEASUREMENT OF GROUP SIZE

In the main body of the paper, we characterize the time-scale of group disruption, $\tau_{\rm d}$, defined as the time taken for a group to double the rms distance of the member galaxies, σ_r, compared to their value at infall. We have experimented with several other definitions to ensure that $\tau_{\rm d}$ is a good measure of the disruption time-scale.

Fig. A1 shows for the example group in Fig. 2, the time evolution of a characteristic (spatial) size defined in several ways: (*i*) σ_r as adopted in the paper (magenta), (*ii*) the average of distances between galaxy members in the group (red), (*iii*) the radius enclosing half of the group members r_{50} (green), or (*iv*) average distances to the centre of mass of the group (blue). All values are shown normalized to its infall value.

As indicated in the figure, all definitions lay very close to each other, a behaviour that is common to all our groups analysed here.

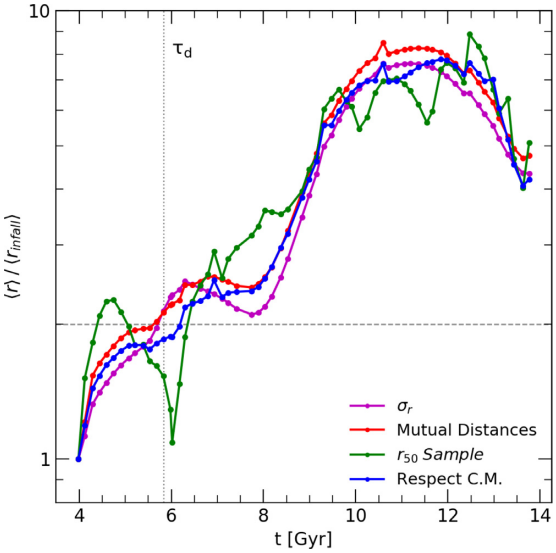

Figure A1. Size evolution with time for one of our infalling groups while it orbits within the host cluster. This group is the same as shown in Fig. 2, lines start at the identified infall time. Different curves correspond to different definition of size (see text for more detail), with magenta being our definition adopted in the paper (the rms distance between galaxies in the group). Curves have been individually normalized to their infall value. All methods give a similar behaviour, with r_{50} (the radius containing half of the group members at different times, shown in green) being slightly more noisy than the rest. Note that the time-scale of disruption $\tau_{\rm d}$, here defined as the time where σ_r has doubled with respect to the infall value (dotted vertical line), would be nearly the same regardless of the specific method chosen to quantify the group size.

More specifically, we use the time $\tau_{\rm d}$ measured as the time when σ_r has doubled its initial value, highlighted by the dotted vertical line, to characterize the spatial disruption time-scale. Any of these methods would have resulted on a very similar time measurement. We therefore adopt $\tau_{\rm d}$ in the remaining of our analysis.

This paper has been typeset from a TEX/LATEX file prepared by the author.